

This is a pre-print version of the paper. Please cite the final version of the paper:

G. Di Martino, A. Iodice, "Orthogonal Coprime Synthetic Aperture Radar", *IEEE Trans. Geosci. Remote Sens.*, vol. 55, no. 1, pp. 432-440, Jan. 2017. DOI: [10.1109/TGRS.2016.2586189](https://doi.org/10.1109/TGRS.2016.2586189).

IEEE Copyright notice. © 2016 IEEE. Personal use of this material is permitted. Permission from IEEE must be obtained for all other uses, in any current or future media, including reprinting/republishing this material for advertising or promotional purposes, creating new collective works, for resale or redistribution to servers or lists, or reuse of any copyrighted component of this work in other works.

Orthogonal Coprime Synthetic Aperture Radar

Gerardo Di Martino, *Member, IEEE*, and Antonio Iodice, *Senior Member, IEEE*

Abstract—Recently, we have proposed a new synthetic aperture radar (SAR) technique, which we called “Coprime SAR” (CopSAR), applicable to the case of bright targets over a dark background and therefore useful in ocean monitoring for ship detection. The CopSAR technique is based on the adaptation of the coprime array beamforming concept to the case of SAR systems, and, in its basic implementation, it is able to reduce the amount of data to be stored and processed, with no geometric resolution loss. A more complex dual-frequency implementation allows us to additionally obtain a significant increase in the range swath size with respect to the standard SAR technique. However, for both practical and theoretical reasons, the simplest single-frequency implementation is preferable. Accordingly, here, we present an enhancement of the CopSAR basic implementation, based on the transmission of (quasi) orthogonal waveforms, i.e., up- and down-chirps: we name it “Orthogonal Coprime SAR” (OrthoCopSAR). The proposed implementation is able to achieve both data reduction and range swath extension with no appearance of ghosts, no resolution loss, and only a limited complication of the required technology. The only costs are the reduction in the target-to-background ratio and the presence of a (nonstringent) limit on maximum ship size, as it is the case in all CopSAR implementations.

Index Terms—Coprime sampling, maritime applications, orthogonal waveforms, synthetic aperture radar (SAR).

I. INTRODUCTION

THE demand for high resolution and coverage of synthetic aperture radar (SAR) systems [1]–[3] for maritime applications implies a huge increase in the amount of data to be stored and processed. Recently, a new technique based on coprime sensing concepts [4], [5] applied to SAR, i.e., Coprime SAR (CopSAR), has been presented [6], and it has been validated by using both simulated and real SAR data [6]. It can be used for scenes consisting of bright targets over a dark (not necessarily homogeneous) background, so that it can be useful in ocean monitoring for ship detection. The CopSAR technique is able to reduce the amount of data and, at the same time, to increase the range swath, with no geometric resolution loss [6]. It has a range of applications similar to that of new SAR processing techniques based on compressive sensing [7]–[9] and shares with them the advantage of a reduction in data amount, but it has the additional advantage of requiring no increase in hardware and processing complexity with respect to standard SAR [6]. The general approach consists in the transmission

of two interlaced sequences of pulses, with two sub-Nyquist pulse repetition frequencies (PRFs) that are equal to the Nyquist PRF divided by two coprime integer numbers. Each sequence is separately processed via standard SAR processing, and the two final aliased (i.e., affected by azimuth ambiguity) images are combined in a very simple way to cancel out aliasing. In particular, three different CopSAR implementations were proposed, aimed at achieving data reduction and/or range swath extension. However, each implementation presents specific drawbacks. The “basic implementation” [6] only allows for data reduction, but it does not support any extension of range swath, which would produce range ambiguity. The “missing-pulse implementation” [6] is useful to reach both aims, but at the cost of the appearance of many (attenuated) ghosts on the image. Finally, the “dual-frequency implementation” [6], which can be also seen as the extension to SAR systems of the direction-of-arrival estimation technique presented in [10], obtains both goals with no appearance of ghosts; however, it requires the use of different frequency bands, thus implying not only a technological complication but also the possible inconvenience of facing different reflectivity patterns in the two aliased images, due to the frequency-dependent behavior of the backscattering coefficient.

In the last years, use of orthogonal transmitted waveforms to mitigate range ambiguity has been proposed in polarimetric SAR [11], high-PRF SAR [12], and MIMO-SAR [13]. Inspired by those works, in this paper, we present an enhancement of the CopSAR basic implementation based on the transmission of (quasi) orthogonal waveforms for the two interlaced sub-Nyquist sequences of pulses, i.e., up- and down-chirps are transmitted in the first and second sequences, respectively. We name this technique *Orthogonal Coprime SAR* (OrthoCopSAR). We show (see Section III) that the combined use of orthogonal waveforms and CopSAR significantly mitigates the drawback of the orthogonal waveform approach highlighted in [14], i.e., the increase in the background noise. The proposed OrthoCopSAR implementation is able to achieve both data reduction and range swath extension by using a single frequency, with no appearance of ghosts, no resolution loss, and only a very limited complication of the required technology. The only costs are the reduction in the target-to-background ratio (TBR) and the presence of a (nonstringent) limit on maximum ship size, as it is the case also for previously presented CopSAR implementations. This very good performance is obtained over the entire scene if two antennas, one transmitting and one receiving, are used. Otherwise, if a single antenna is used for both transmission and reception, there will be a strip, corresponding to “blind ranges” of some of the pulses, in which a moderate ambiguity is present, as detailed in Section III.

This paper is organized as follows. In Section II, azimuth and range ambiguity phenomena and the CopSAR concept are briefly recalled. In Section III, the rationale of the proposed OrthoCopSAR technique is presented, and single- and

Manuscript received January 26, 2016; revised May 2, 2016 and July 25, 2016; accepted September 8, 2016.

The authors are with the Dipartimento di Ingegneria Elettrica e delle Tecnologie dell’Informazione, Università di Napoli Federico II, 80125 Napoli, Italy (e-mail: gerardo.dimartino@unina.it; iodice@unina.it).

Color versions of one or more of the figures in this paper are available online at <http://ieeexplore.ieee.org>.

Digital Object Identifier 10.1109/TGRS.2016.2608140



Fig. 1. CopSAR concept, $N_1 = 4$, $N_2 = 5$: locations along the SAR line of flight at which pulses are transmitted. (Blue) First sequence. (Red) Second sequence. (White) Pulse not transmitted.

dual-antenna implementations are discussed. In Section IV, meaningful experiments on simulated data are presented. Finally, conclusions are reported in Section V.

II. THEORETICAL BACKGROUND

A. Azimuth and Range Ambiguity

Due to the finite value of the PRF, replicas of the reflectivity pattern may appear on SAR images, and this phenomenon is usually referred to as azimuth ambiguity [15] or aliasing. Such replicas are shifted both in azimuth and, although in a smaller extent, in range. In particular, the azimuth and range shifts of the i th replica are [15], [16]

$$\Delta x_i = i \frac{\text{PRF} \lambda r_0}{2v} \quad \Delta r_i = \frac{\Delta x_i^2}{2r_0} \quad (1)$$

where λ is the electromagnetic wavelength, r_0 is the closest range between the platform and the center of the real antenna footprint, and v is the sensor velocity. However, these replicas are slightly defocused for $i \neq 0$, and they are weighted by the real antenna azimuth pattern (AAP). In standard SAR systems, the PRF is chosen in such a way that

$$|\Delta x_1| > X, \quad \text{i.e.,} \quad \frac{\text{PRF} \lambda r_0}{2v} \geq x, \quad \text{i.e.,} \quad \text{PRF} \geq \frac{2v}{L} \quad (2)$$

where $X = \lambda r_0 / L$ is the real antenna footprint azimuth size, with L being the real antenna azimuth length (it can be also verified that condition (2) is actually the Nyquist condition for the SAR signal azimuth sampling); therefore, assuming an ideal AAP that is null outside its main beam (i.e., that has no sidelobes), all replicas are suppressed, and only the actual targets appear on the image. In practice, the ideal AAP condition can be only approached by using an antenna with a high peak-to-sidelobe ratio, but it can never be exactly achieved. However, replicas outside the AAP main beam are strongly attenuated, and they can be neglected, apart from some particular cases, for which techniques are available to strongly reduce them [15], [16].

However, for very high resolution SAR systems, condition (2) corresponds to a very high value of the PRF, and this, on one hand, implies that a large amount of data has to be stored and processed and, on the other hand, poses a strict limit on the scene range size. In fact, to avoid range ambiguity, i.e., partial overlapping of subsequent received pulses, the scene slant range size cannot exceed the value

$$W_{\max} = \frac{c}{2}(\text{PRI} - 2\tau) \quad (3)$$

where c is the speed of light, τ is the chirp duration, and $\text{PRI} = 1/\text{PRF}$ is the pulse repetition interval.

B. Coprime SAR

To solve both problems previously mentioned, at least for scenes consisting of bright targets over a dark (not necessarily

homogeneous) background, we have recently proposed the CopSAR technique [6]. In this new acquisition mode, the system transmits two interlaced sequences of pulses: one at $\text{PRF}_1 = \text{PRF}_0 / N_1$ and the other at $\text{PRF}_2 = \text{PRF}_0 / N_2$, where PRF_0 satisfies condition (2), i.e., $\text{PRF}_0 \geq 2v/L$, and N_1 and N_2 are two coprime integers (i.e., their greatest common divisor is 1). This is realized by transmitting pulses at times $t_n = n/\text{PRF}_0$ only if n is an integer multiple of N_1 or N_2 (i.e., $n = n_1 N_1$ or $n = n_2 N_2$, with n_1 and n_2 integers), instead that for all integer values of n , as it is the case for the standard acquisition mode (see Fig. 1). The two sequences can be separately processed to obtain two SAR images, i.e., $s_1(x, r)$ and $s_2(x, r)$. Here, x and r are the azimuth and range coordinates, respectively. The geometric resolution of these images will not be changed with respect to the standard SAR case, because the synthetic array length (i.e., the processed azimuth bandwidth) is unchanged, but of course, these images will be severely aliased. However, if the scene consists of bright targets on a dark background (as in the case of boats or ships on the ocean), then only the true targets will be present on both aliased images at the same location, whereas aliased targets (i.e., replicas) will be at different locations on the two images. In fact, spacings of target replicas on images $s_1(x, r)$ and $s_2(x, r)$ are

$$\Delta x_{i_1} = i_1 \frac{\text{PRF}_0 \lambda r_0}{N_1 2v} \quad \Delta x_{i_2} = i_2 \frac{\text{PRF}_0 \lambda r_0}{N_2 2v} \quad (4)$$

respectively, with i_1 and i_2 integers, so that replicas on the two images will not be at the same location unless $i_1/i_2 = N_1/N_2$. Since N_1 and N_2 are coprime, this only happens if $i_1 = iN_1$ and $i_2 = iN_2$, so that

$$\Delta x_{i_1} = \Delta x_{i_2} = i \frac{\text{PRF}_0 \lambda r_0}{2v} \quad (5)$$

i.e., only at the positions of the replicas in the image that would be obtained in the standard acquisition mode [see (1)]. Since $\text{PRF}_0 \geq 2v/L$, these replicas are suppressed (actually, strongly attenuated) by the AAP. Therefore, using the simple combination rule

$$s(x, r) = \begin{cases} s_1(x, r), & \text{if } |s_1(x, r)| < |s_2(x, r)| \\ s_2(x, r), & \text{otherwise} \end{cases} \quad (6)$$

we obtain a final image $s(x, r)$ in which no replicas are present. As a matter of fact, where in one of the two images there is a target replica, in the other one there is only the sea background, and in selecting the smallest amplitude we correctly select the sea background. Conversely, where the true target is present, both images have similar high amplitudes, and even in selecting the smallest amplitude we correctly obtain a brilliant pixel.

The data rate reduction with respect to the standard SAR acquisition mode, the maximum range swath extension factor, and the minimum distance Δ_{\min} between consecutive replicas on the two aliased images have been computed in [6] for the

TABLE I
TECHNIQUE PERFORMANCE INDICATORS

Configuration	Data rate reduction factor	Maximum range swath extension factor	Maximum azimuth target size (Δ_{min})
CopSAR basic	$\frac{N_1 + N_2 - 1}{N_1 N_2}$	1	$\frac{PRF_0 \lambda r_0}{N_1 N_2 2v}$
CopSAR missing pulse	$\frac{N_1 + N_2 - 3}{N_1 N_2}$	2	$\frac{PRF_0 \lambda r_0}{N_1 N_2 2v}$
CopSAR dual frequency	$\frac{2}{N_1}$	N_1 (single antenna: $N_1/2$)	$\frac{PRF_0 \lambda r_0}{N_1 N_2 2v}$
OrthoCopSAR	$\frac{N_1 + N_2}{N_1 N_2}$	N_1	$\frac{PRF_0 \lambda r_0}{N_1 N_2 2v}$

different CopSAR implementations, and they are listed in the first three rows of Table I. The value of Δ_{min} limits the allowed azimuth size of the bright targets [6], so that it sets a tradeoff between data amount reduction, for which high values of N_1 and N_2 are desirable, and maximum azimuth size of targets, which increases if N_1 and N_2 are decreased. Another factor that limits the values of N_1 and N_2 is the TBR over the final CopSAR image, which is reduced by a factor on the order of $N_2^2/(N_1 + N_2)$ with respect to the standard SAR image [6]. For $N_2 = N_1 + 1$, which is the choice suggested in [6], this corresponds to about $N_2/2$.

III. ORTHOGONAL COPRIME SAR

The direct implementation of the above-described concept (i.e., the “basic implementation,” see [6]) only reduces the amount of data to be stored and processed, but it does not allow for an extension of the range swath, because the minimum time separation between consecutive pulses is $1/PRF_0$, as in the case of standard SAR. However, at variance with the standard SAR case, this minimum separation only occurs twice every $N_1 + N_2$ pulses. Therefore, when the range swath size exceeds $c \text{ PRI}_0/2$, range ambiguity affects standard and coprime SAR systems in different ways. In fact, in the standard SAR case, range-shifted replicas of true targets will appear, with intensity similar to that of the true targets (a small attenuation is due to the slight defocusing). Conversely, in the coprime SAR case, range-shifted replicas will be significantly attenuated with respect to the true targets, because only some of the pulses will be affected by range ambiguity (this further amplitude attenuation factor is N_2 , see below); however, this will introduce an azimuth periodicity, with frequency on the order of $PRF_0/(N_1 N_2)$, that causes the appearance of attenuated azimuth replicas. This will be illustrated with numerical examples in Section IV. Accordingly, no extension of the range swath is possible for the CopSAR basic implementation. To overcome this problem, we here propose a technique, which we name OrthoCopSAR, that differs from standard CopSAR in the fact that pulses of the two interlaced subsampled sequences are mutually (quasi) orthogonal: In the first subsampled sequence, up-chirp waveforms are transmitted, whereas in the second subsampled sequence, down-chirp waveforms are used (when the two sequences superimpose, i.e., first and last pulse in Fig. 1, the two waveforms are summed up and transmitted). Since up-

chirp and down-chirp waveforms are quasi-orthogonal¹ [14], nonaliased images can be still obtained processing each sequence via the appropriate up- or down-chirp matched filtering during range compression. The energy of the unfocused target contribution, due to the presence of the mismatched chirp, will be spread over twice the entire pulse duration interval in the final focused image [14]. It is important to note that in the OrthoCopSAR case, superposition at the receiver of focused and unfocused contributions is only partial, and it does not happen for all pulses. To see this, let us first consider the case in which the range swath is larger than $c/2$ times PRI_0 , but smaller than c times PRI_0 (i.e., it is approximately doubled with respect to the standard SAR case): In this case, superposition is present only for pulses of the two subsequences transmitted at the same time or at distance $1/PRF_0$, i.e., three times out of $N_1 + N_2$. Accordingly, the corresponding reduction in radiometric resolution (as predicted by the analysis in [14]) will be negligible in the OrthoCopSAR case, and the reduction in the TBR is expected to be similar to that of the CopSAR basic implementation [6]. This expectation is confirmed by experiments (see Section IV). Let us now move to consider the case of range swath larger than twice the standard SAR range swath. As the range swath size increases, the number of pulses affected by superposition of focused and unfocused contributions increases. The maximum range swath extension factor that prevents the appearance of range ambiguity is N_1 for the OrthoCopSAR case, but in this case, all pulses are affected by superposition of focused and unfocused contributions, and an increase in background noise is expected. However, it can be verified that if at any equi-azimuth line there is only one bright target and if (as is usually the case in standard SAR systems) $2\tau < \text{PRI}_0$, then in each cycle of duration $N_1 N_2 \text{PRI}_0$, range-ambiguous unfocused contributions affect different pulses of each sequence in different range intervals, so that each range interval is only affected by a range-ambiguous unfocused contribution in two pulses out of $N_1 + N_2$. Therefore, if the scene includes a few bright targets over a darker background, even for the maximum range swath extension factor, the reduction in the TBR for the OrthoCopSAR is expected to be similar to that of the CopSAR basic implementation. Accordingly, it can be concluded that

¹Up-chirp and down-chirp may be slightly modified to obtain perfectly orthogonal waveforms via a simple procedure described in [14]; however, corresponding improvement is so small that the procedure is not worth being implemented [14].

the presented OrthoCopSAR technique also allows obtaining a wider range swath, in addition to the reduction in the number of transmitted pulses. The data rate reduction, the maximum range swath, and the maximum target azimuth size for the OrthoCopSAR case can be easily computed, and they are listed in the fourth row of Table I. In addition, in view of the considerations previously reported, the attenuation of the range ambiguity of a bright target can be theoretically computed. In fact, since the energy of the ambiguous target is spread over twice the entire pulse duration interval, a first power attenuation factor is present, which is equal to the ratio between $c\tau$ and the slant range resolution $c/(2B)$, where B is the chirp bandwidth. In addition, a further power attenuation factor is due to the fact that in each cycle of duration $N_1 N_2 \text{PRI}_0$, range-ambiguous unfocused contributions affect different pulses of each sequence in different range intervals. In view of the combination rule of (6), this further power attenuation factor is N_2^2 . Accordingly, the overall range ambiguity power attenuation factor is

$$R_{ra} = 2\tau B N_2^2. \quad (7)$$

It may be noted that a wider swath implies a wider antenna beam, which, in turn, corresponds to a smaller antenna gain; accordingly, a lower signal-to-noise ratio (SNR; with respect to thermal noise) is obtained. However, in modern SAR systems, the thermal noise level is so small that a reduction in SNR of even one order of magnitude is not an issue for a bright target such as a ship or a boat. In addition, the reduction in SNR can be at least partly compensated for by increasing the transmitted pulse peak power, without increasing the transmitted average power, since the number of transmitted pulses is reduced.

The best way to implement an OrthoCopSAR system is to use two antennas, i.e., one transmitting and one receiving. However, the proposed technique can be also implemented on single-antenna SAR sensors. In this case, “blind ranges” (i.e., $c\tau$ -wide ground strips from which no signal is available) are present in the raw signal, due to the fact that the sensor cannot receive during the transmission interval. However, when doubling the range swath, this only happens for pulses at distance $1/\text{PRF}_0$ (i.e., two out of $N_1 + N_2$). Therefore, on the final image, this implies no blind range, but only the possible appearance of strongly attenuated azimuth replicas, similar to those arising in the CopSAR missing-pulse implementation [6], over a specific slant range interval of size equal to $c\tau$. If the range swath size further increases, blind ranges appear also in consecutive pulses at distances larger than $1/\text{PRF}_0$; however, it can be verified that in each cycle of duration $N_1 N_2 \text{PRI}_0$, blind ranges appear in different range positions in different pulses of each sequence, so that each range interval can be “blind” in no more than two pulses out of $N_1 + N_2$. Accordingly, even for the maximum range swath extension factor N_1 , on the final image, this implies no blind range, but only the possible appearance of strongly attenuated azimuth replicas, similar to those arising in the CopSAR missing-pulse implementation, over specific (no more than $N_1 - 1$) slant range intervals of size equal to $c\tau$.

We want to stress at this point that although it may seem that the OrthoCopSAR operation implies solving an involved timing problem, the latter actually turns out to be quite simple if we see it as the combination of two periodic timings, one for each subsequence. Accordingly, a simple control logic is needed to implement the rules for the selection of pulse transmission

TABLE II
SIMULATION PARAMETERS

Platform height	[km]	224
Platform velocity	[km/s]	7.7
Look angle	[°]	35
Azimuth antenna size	[m]	8.6
Range antenna size	[m]	0.5 (0.25)
Carrier frequency	[GHz]	1.282
Pulse duration	[μs]	30.4 (50)
Chirp bandwidth	[MHz]	12 (4.7)
Sampling rate	[Mhz]	12 (4.7)
PRF ₀	[Hz]	2800
Doppler centroid	[Hz]	0

This Table refers to the case of doubled range swath, except for the values reported in parenthesis that are relevant to the case of range-swath size increased by a factor $N_1=5$.

times, of receiving windows, and of the proper sections (i.e., the echoes of each transmitted pulse) of the received registered signal to be processed with the two matched filters.

Finally, it is worth mentioning that, as in the CopSAR case, also for OrthoCopSAR systems, the condition on the maximum target azimuth size can be relaxed by computing the correlation coefficient between $s_1(x, r)$ and $s_2(x, r)$ over a window in correspondence of each bright spot of $s(x, r)$ and retaining as valid bright spots only those corresponding to a nearly unitary correlation coefficient [6]. This also solves for the very unfortunate circumstance that a replica of one target in the image $s_1(x, r)$ overlaps with a replica of another target in the image $s_2(x, r)$, thus causing the appearance, on the combined image $s(x, r)$, of a “ghost,” i.e., of a false bright target [6]. This solution, already suggested in [6], leads to low false-alarm rates, but it is not fully automated, since it requires user intervention in the selection of windows on which to compute the correlation coefficient. Conversely, based on the same concept, we here suggest the following fully automatic OrthoCopSAR-based ship detection strategy. The two aliased images $s_1(x, r)$ and $s_2(x, r)$, in addition to be combined by using (6) to generate the OrthoCopSAR image $s(x, r)$, are also used to generate a correlation coefficient (or *coherency*) map $c(x, r)$, i.e.,

$$c(x, r) = \frac{\langle s_1(x, r) s_2^*(x, r) \rangle}{\sqrt{\langle |s_1(x, r)|^2 \rangle \langle |s_2(x, r)|^2 \rangle}} \quad (8)$$

where $\langle \cdot \rangle$ stands for the average over an $n \times n$ window centered on the considered pixel x, r .

The final image, in which the ghosts are “cleaned up,” is finally obtained by multiplying $s(x, r)$ by $c^2(x, r)$, where the square is considered to increase ghost damping. This image can be used as input for a standard ship detection algorithm. Note that such final image retains the full geometric resolution of $s(x, r)$, whereas in the coherency map $c(x, r)$, the geometric resolution is worsened by a factor n . An example of application of such a strategy will be reported in Section IV, in which a proper choice for the window size n will be suggested.

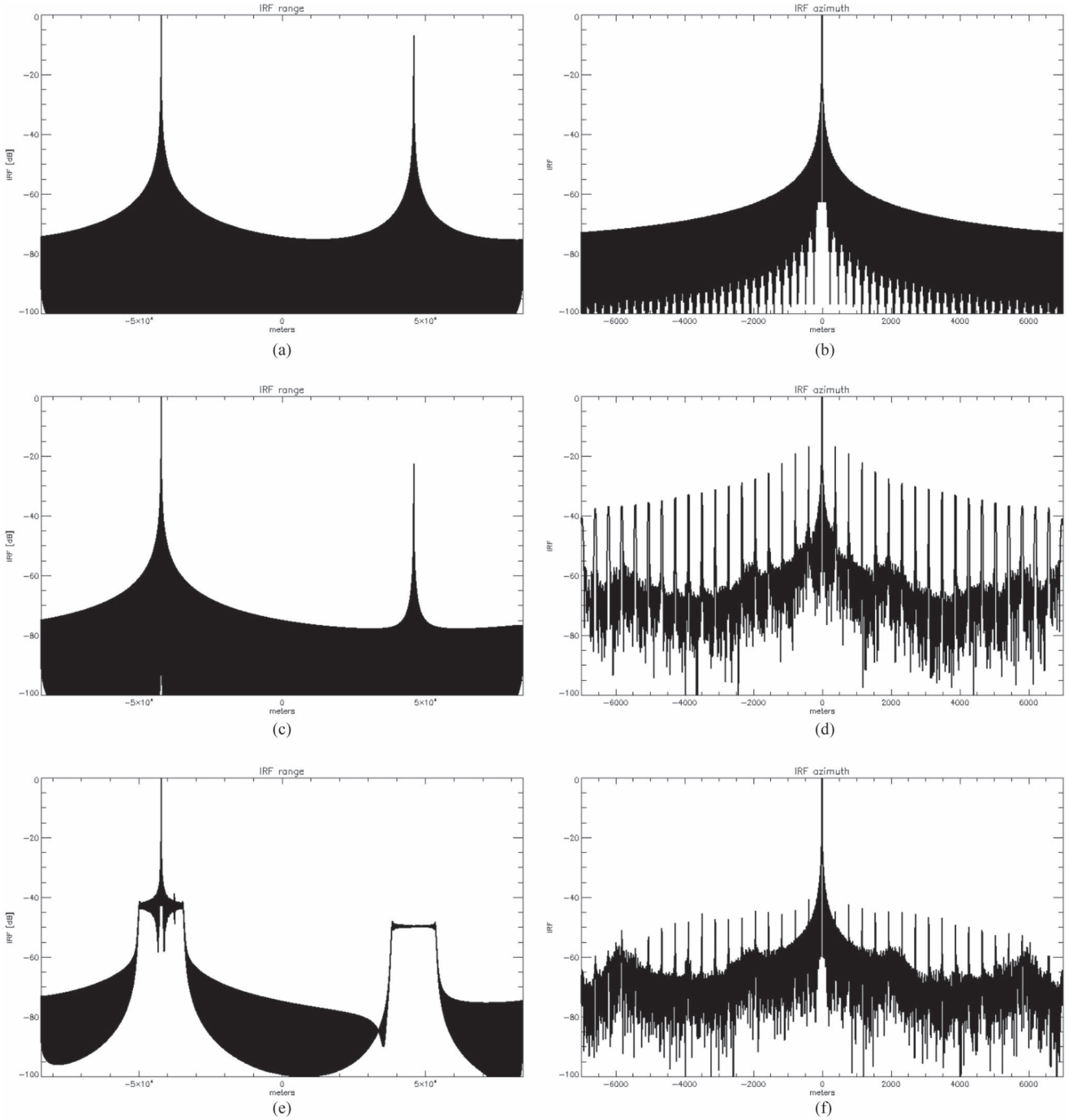


Fig. 2. Plots of (a), (c), and (e) range and (b), (d), and (f) azimuth IRFs normalized to their maximum value for (a) and (b) the standard SAR case, (c) and (d) the standard CopSAR case, and (e) and (f) the OrthoCopSAR case.

IV. EXPERIMENTAL RESULTS

In this section, we test the proposed approach by applying it to simulated SAR raw signals. All the employed SAR raw signals have been generated using the SAR raw signal simulator in [17] and [18] and have been focused via the Fourier-domain SAR processor described in [2]. The considered SAR system parameters are listed in Table II. Note that, for this system, condition (3) is not satisfied; in fact, the range swath is about 160 km, i.e., about twice the size of the maximum swath allowed according to condition (3). Consequently, range ambiguity is expected to appear for standard SAR and CopSAR acquisition modes.

First of all, to analyze the system amplitude impulse response function (IRF), we consider a scene consisting of a single pointlike target. In all the following examples, we assume $N_1 = 5$ and $N_2 = 6$. The performed simulations are relevant to standard SAR, standard CopSAR, and OrthoCopSAR cases. The obtained results are shown in Fig. 2. In particular, the standard SAR case range and azimuth IRFs are reported in Fig. 2(a) and (b): As expected, the occurrence of range ambiguity can be observed in the range IRF of Fig. 2(a). The amplitude of the ambiguous signal is about 6 dB lower than that of the true target, due to nonperfect focusing. In the standard CopSAR IRF,

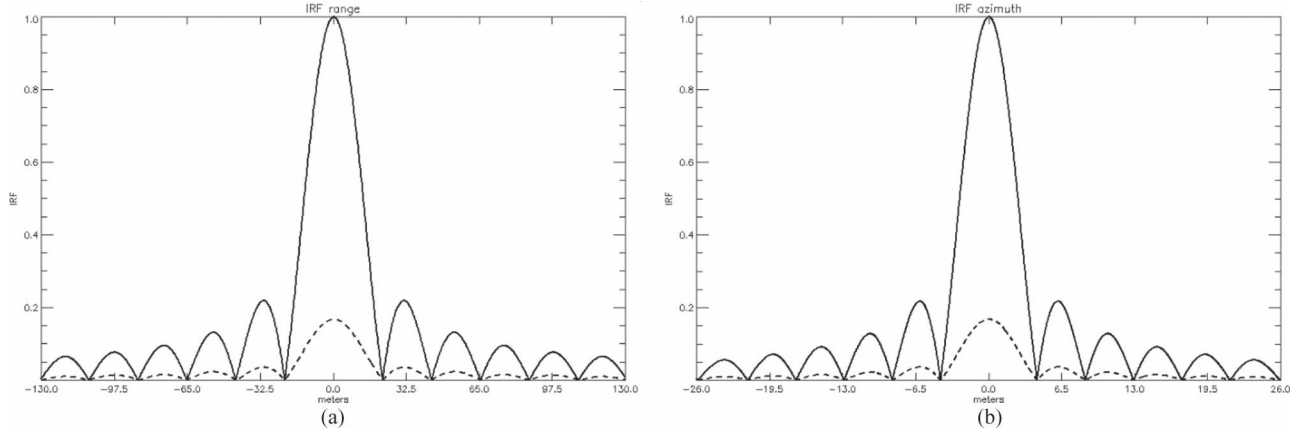


Fig. 3. Enlarged view of (a) range and (b) azimuth IRFs of (continuous line) standard SAR and (dashed line) OrthoCopSAR implementations, normalized to the maximum value of the standard SAR IRF.

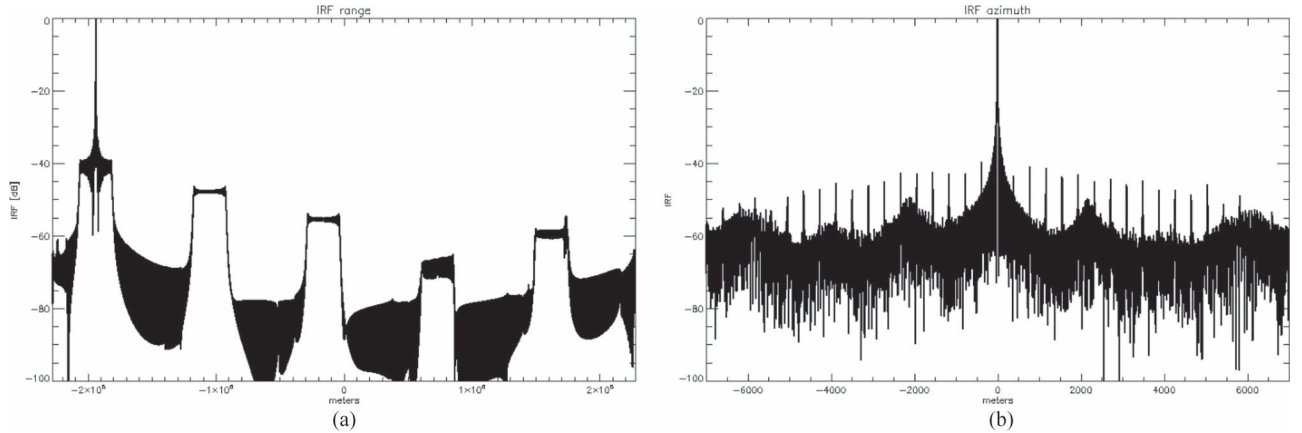


Fig. 4. Plots of (a) range and (b) azimuth IRFs normalized to their maximum value for OrthoCopSAR with range swath size increased by a factor $N_1 = 5$.

the range ambiguity is still present: However, the amplitude of the ambiguous signal is reduced by about 21 dB (i.e., of an additional factor $N_2 = 6$, corresponding to about 15 dB, as theoretically predicted in Section III), due to the limited number of pulses affected by range ambiguities [see Fig. 2(c)]. As discussed in the previous section, however, the presence of the periodicity related to the pulses affected by range ambiguity is responsible for the appearance of azimuth ambiguities: The peak amplitude of these ambiguities is about -15 dB with respect to the amplitude of the true target [see Fig. 2(d)]. Both range and azimuth ambiguities are almost removed using the OrthoCopSAR implementation, as testified by Fig. 2(e) and (f), where the level of the residual ambiguity is less than -40 dB. As expected, in the range IRF of Fig. 2(e), the energy of the unfocused contributions is spread over twice the pulse duration, and the residual range ambiguity level is attenuated with respect to the standard SAR case of about -44 dB, which is the theoretical value predicted by (7). Finally, to verify the absence of resolution loss in the OrthoCopSAR case in Fig. 3, we show enlarged views of range and azimuth IRFs centered on the target, which allow us to appreciate how the width of the main lobe is the same in the standard and OrthoCopSAR cases, whereas its amplitude decreases by a factor $1/N_2 = 1/6$, as theoretically expected.

To demonstrate the maximum increase in the range swath size attainable with the OrthoCopSAR approach, in Fig. 4, we

report the range and azimuth IRFs obtained for an increase by a factor $N_1 = 5$. Some of the parameters used for this simulation have been accordingly modified in such a way as to obtain a range swath size five times larger than the maximum swath allowed by condition (3). The modified parameter values are reported in parentheses in Table II. As theoretically expected, in Fig. 4, it can be appreciated that the level of residual ambiguity is less than -40 dB. In particular, also in this case for all the four range ghosts present on the scene, the residual ambiguity level is lower than -42 dB, which is the theoretical value predicted by (7) with the new parameters.

Now, we move to a more complex scene composed of two very large ships (whose reflectivity functions have been obtained from an actual SAR image) over a uniform speckled dark background: One of the ships is oriented along the range direction, whereas the other presents a 45° angle with respect to the range direction. Moreover, in the following examples, we use for the CopSAR and OrthoCopSAR implementations $N_1 = 5$ and $N_2 = 6$. The obtained results are shown in Fig. 5, where an appropriate spatial multilook has been performed, thus obtaining an approximately square pixel. In Fig. 5(a), the image resulting in the standard SAR case is reported: As expected, range ambiguity is present. The true ships are those located in near range. Note that a region with a darker background is present at middle range, where nonambiguous and range-ambiguous focused signals are not overlapped.

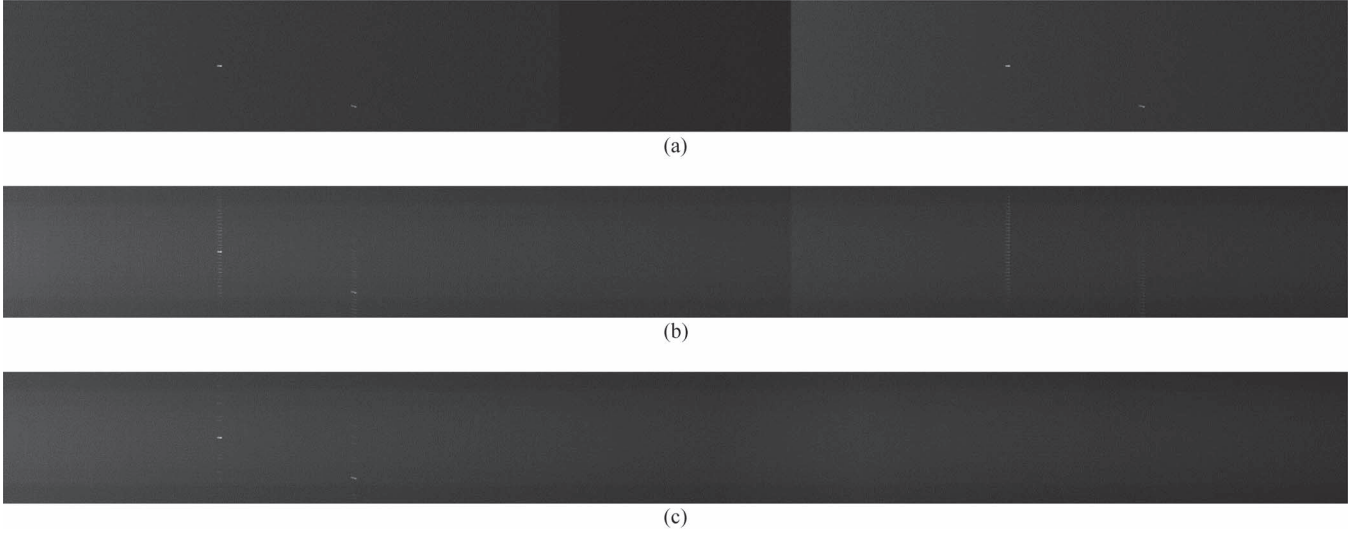


Fig. 5. Simulation results. (a) Standard SAR case. (b) Standard CopSAR case. (c) OrthoCopSAR case. Near range is on the left.



Fig. 6. Simulation results. OrthoCopSAR case with a ship placed in the region influenced by "blind ranges." Near range is on the left.

The result obtained with the application of the standard basic CopSAR implementation is presented in Fig. 5(b). In this case, attenuated azimuth replicas of the true target are still visible. Moreover, attenuated range ambiguities and associated azimuth ambiguities of the range ghost ships are also visible in the far range of the image. All these phenomena are consistent with the above reported IRF analysis.

In Fig. 5(c), we show the image obtained applying the OrthoCopSAR implementation: In this case, only a very low residual azimuth ambiguity is (hardly) visible, while no range ambiguity can be appreciated. Note that the reduction in the TBR with respect to the standard SAR case is equal to about 2.1, and it is almost the same for both the standard CopSAR and OrthoCopSAR cases: This value is significantly lower than the approximate theoretical one computed as in [6], which, in this case, is equal to about $N_2/2 = 3$. Finally, to provide an example of the effects related to the presence of "blind ranges" on the raw signal, in Fig. 6, we show the result of the application of the OrthoCopSAR implementation for a scene consisting of a ship placed in the image area affected by "blind ranges." As theoretically expected, in this situation, strongly attenuated azimuth replicas of the ship, similar to those obtained in the CopSAR missing-pulse implementation [6], can be appreciated.

To better show that the OrthoCopSAR approach implies no resolution loss, in Fig. 7, we compare the enlarged view of the ship (the minimum spatial multilook necessary to obtain square pixels has been performed) obtained by using standard SAR [see Fig. 7(a)] and OrthoCopSAR [see Fig. 7(b)]. It is evident that the ship details appearing in the standard SAR image are retained in the OrthoCopSAR one. The expected reduction in the TBR, i.e., of the contrast, with respect to the background, in the OrthoCopSAR case is also evident.

We then analyze the performance of the OrthoCopSAR approach in the presence of a nonuniform speckled background.



Fig. 7. Zoomed-in view of one of the ships in Fig. 5 for (a) standard SAR and (b) OrthoCopSAR.

More specifically, the reflectivity function of the same ships used in the previous examples is superimposed on the reflectivity of a typical ocean surface (where an ocean swell pattern is present), obtained using the simulator of maritime scenes described in [18]. The parameters used for the simulations are those reported in Table II. In Fig. 8, we show the results obtained in the standard SAR and OrthoCopSAR cases: We report both the near-range regions, where the actual ships are located, and the far-range regions, where, for standard SAR, range ambiguities are present. As expected, these ambiguities are effectively suppressed by the OrthoCopSAR approach. Moreover, it can be noted that in the OrthoCopSAR image, the visibility of the swell is attenuated, due to the effects of the CopSAR combination rule [6], and therefore, the background tends to be more uniform than in the standard SAR case.

In the last simulated scenario, we demonstrate the use of the correlation coefficient map to reduce the presence of residual ambiguity, considering the case of a ship aligned to the azimuth whose azimuth size exceeds Δ_{\min} . As shown in Fig. 9(a), in this case, azimuth ambiguity is present on the OrthoCopSAR

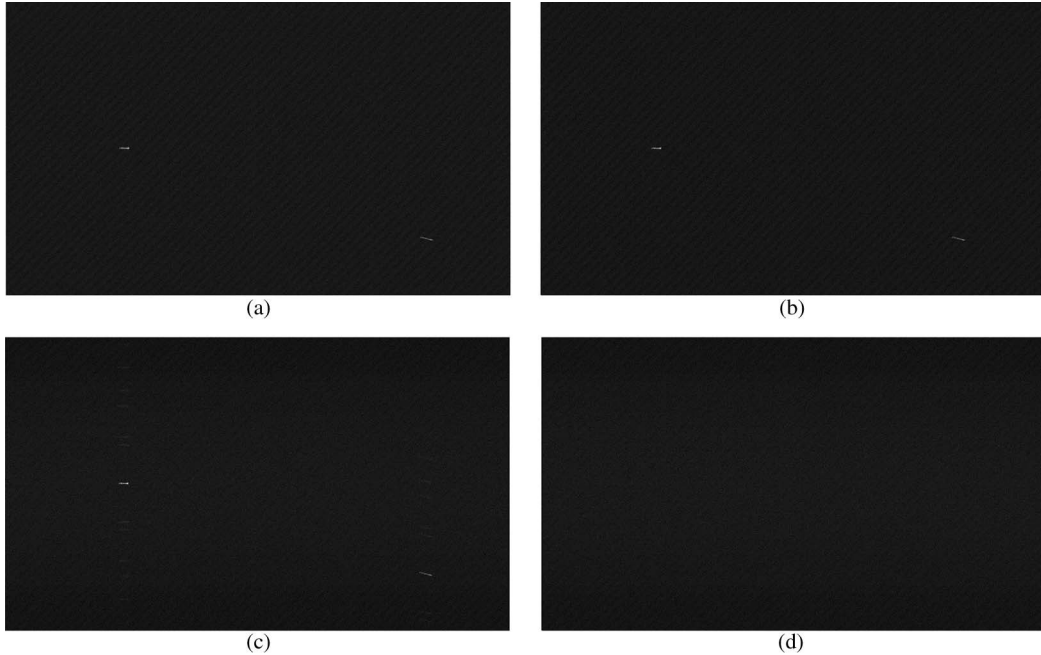


Fig. 8. Simulation results in the presence of ocean swell. (a) Standard SAR case in near range (actual ships). (b) Standard SAR case in far range (range ambiguity is visible). (c) OrthoCopSAR case in near range (actual ships). (d) OrthoCopSAR case in far range (range ambiguity is not visible). Near range is on the left.

image. To mitigate this phenomenon, we used (8) to evaluate the correlation coefficient map $c(x, r)$: In particular, we chose to set $n = 4$, which represents a good tradeoff between accuracy of the correlation estimates and resolution of the obtained correlation map. We then multiplied the OrthoCopSAR image by c^2 : The obtained result is reported in Fig. 9(b), where residual ambiguity can be hardly appreciated. In addition, it can be noted that fine details of the ship are preserved, this showing that the full resolution of $s(x, r)$ is maintained in the “cleaned up” image.

V. CONCLUSION

In this paper, an enhancement of the recently introduced CopSAR technique has been presented. It is based on the transmission of (quasi) orthogonal waveforms (namely, up- and down-chirps) for the two sub-Nyquist sequences of pulses transmitted by the CopSAR sensor, and therefore, it has been here called Orthogonal Coprime SAR. The proposed technique is suitable for application to ship detection. In fact, it has been shown that, for a scene consisting of a few bright targets over a darker background, the use of two interlaced sequences of pulses, with two sub-Nyquist PRFs that are equal to the Nyquist PRF divided by two coprime integer numbers, allows us to avoid azimuth ambiguity even in cases in which condition (2) is not satisfied and that the use of up- and down-chirps for the two sequences of pulses allows us to avoid range ambiguity even in cases in which condition (3) is not satisfied. Accordingly, the proposed implementation is able to achieve both data reduction and range swath extension by using a single frequency, with no appearance of ghosts, no resolution loss, and only a very limited complication of the required technology. The only limitations are those intrinsic to any CopSAR implementation: a reduction in the TBR and the presence of a (nonstringent) limit on maximum ship size. The performance of the algorithm has been tested on simulated SAR signals.

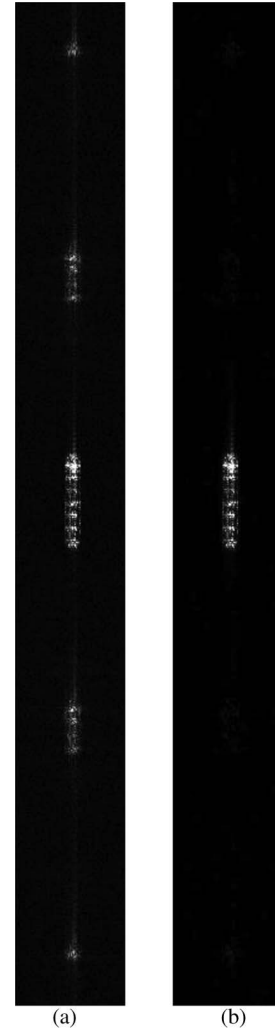


Fig. 9. Simulation results in the presence of a ship aligned along the azimuth and presenting an azimuth size larger than Δ_{\min} . (a) Standard OrthoCopSAR result. (b) Result after multiplication by $c^2(x, r)$.

REFERENCES

- [1] J. C. Curlander and R. N. McDonough, *Synthetic Aperture Radar: Systems and Signal Processing*. New York, NY, USA: Wiley, 1991.
- [2] G. Franceschetti and R. Lanari, *Synthetic Aperture Radar Processing*. New York, NY, USA: CRC Press, 1999.
- [3] A. Moreira, P. Prats-Iraola, M. Younis, G. Krieger, I. Hajnsek, and K. P. Papathanassiou, "A tutorial on synthetic aperture radar," *IEEE Geosci. Remote Sens. Mag.*, vol. 1, no. 1, pp. 6–43, Mar. 2013.
- [4] P. P. Vaidyanathan and P. Pal, "Sparse sensing with co-prime samplers and arrays," *IEEE Trans. Signal Process.*, vol. 59, no. 2, pp. 573–586, Feb. 2011.
- [5] P. P. Vaidyanathan and P. Pal, "Theory of sparse coprime sensing in multiple dimensions," *IEEE Trans. Signal Process.*, vol. 59, no. 8, pp. 3592–3608, Aug. 2011.
- [6] G. Di Martino and A. Iodice, "Coprime Synthetic Aperture Radar (CopSAR): A new acquisition mode for maritime surveillance," *IEEE Trans. Geosci. Remote Sens.*, vol. 53, no. 6, pp. 3110–3123, Jun. 2015.
- [7] M. Tello Alonso, P. López-Dekker, and J. J. Mallorquí, "A novel strategy for radar imaging based on compressive sensing," *IEEE Trans. Geosci. Remote Sens.*, vol. 48, no. 12, pp. 4285–4295, Dec. 2010.
- [8] V. M. Patel, G. R. Easley, D. M. Healy, and R. Chellappa, "Compressed synthetic aperture radar," *IEEE J. Sel. Topics Signal Process.*, vol. 4, no. 2, pp. 244–254, Apr. 2010.
- [9] J. Fang, Z. Xu, B. Zhang, W. Hong, and Y. Wu, "Fast compressed sensing SAR imaging based on approximated observation," *IEEE J. Sel. Topics Appl. Earth Observ. Remote Sens.*, vol. 7, no. 1, pp. 352–363, Jan. 2014.
- [10] M. G. Amin, "Sufficient conditions for alias-free direction of arrival estimation in periodic spatial spectra," *IEEE Trans. Antennas Propag.*, vol. 41, no. 4, pp. 508–511, Apr. 1993.
- [11] J. Kim, M. Younis, A. Moreira, and W. Wiesbeck, "A novel OFDM waveform for fully polarimetric SAR data acquisition," in *Proc. EUSAR*, Aachen, Germany, 2010, pp. 1–4.
- [12] W.-Q. Wang, "Mitigating range ambiguities in high-PRF SAR with OFDM waveform diversity," *IEEE Geosci. Remote Sens. Lett.*, vol. 10, no. 1, pp. 101–105, Jan. 2013.
- [13] W.-Q. Wang, "Space–time coding MIMO-OFDM SAR for high-resolution imaging," *IEEE Trans. Geosci. Remote Sens.*, vol. 49, no. 8, pp. 3094–3104, Aug. 2011.
- [14] G. Krieger, "MIMO-SAR: Opportunities and pitfalls," *IEEE Trans. Geosci. Remote Sens.*, vol. 52, no. 5, pp. 2628–2645, May 2014.
- [15] R. K. Raney and G. J. Princz, "Reconsideration of azimuth ambiguities in SAR," *IEEE Trans. Geosci. Remote Sens.*, vol. 25, no. 6, pp. 783–787, Nov. 1987.
- [16] G. Di Martino, A. Iodice, D. Riccio, and G. Ruello, "Filtering of azimuth ambiguity in stripmap synthetic aperture radar images," *IEEE J. Sel. Topics Appl. Earth Observ. Remote Sens.*, vol. 7, no. 9, pp. 3967–3978, Sep. 2014.
- [17] G. Franceschetti, M. Migliaccio, D. Riccio, and G. Schirrinzi, "SARAS: A SAR raw signal simulator," *IEEE Trans. Geosci. Remote Sens.*, vol. 30, no. 1, pp. 110–123, Jan. 1992.
- [18] G. Franceschetti, A. Iodice, D. Riccio, G. Ruello, and R. Siviero, "SAR raw signal simulation of oil slicks in ocean environments," *IEEE Trans. Geosci. Remote Sens.*, vol. 40, no. 9, pp. 1935–1949, Sep. 2002.



Gerardo Di Martino (S'06–M'09) was born in Naples, Italy, on June 22, 1979. He received the Laurea degree (*cum laude*) in telecommunication engineering and the Ph.D. degree in electronic and telecommunication engineering from the University of Naples Federico II, Naples, in 2005 and 2009, respectively.

During 2009–2016, he was with the University of Naples Federico II, working on several research projects regarding indoor electromagnetic propagation and localization of unknown transmitters, information extraction from high-resolution SAR images of natural and urban areas, maritime surveillance with SAR data, and sparse antenna arrays. During 2014–2015, he conducted research in the field of electromagnetic propagation in harbor scenarios and innovative network architectures through Grants received from the Italian National Consortium for Telecommunications. He is currently with the Department of Electrical Engineering and Information Technology, University of Naples Federico II, working on a project regarding forward-looking SAR systems. His main research interests include microwave remote sensing and electromagnetics, with particular focus on the modeling of electromagnetic scattering from natural surfaces and urban areas, SAR signal processing and simulation, information retrieval from SAR data, and remote sensing techniques for developing countries.



Antonio Iodice (S'97–M'00–SM'04) was born in Naples, Italy, in 1968. He received the Laurea degree (*cum laude*) in electronic engineering and the Ph.D. degree in electronic engineering and computer science from the University of Naples Federico II, Naples, in 1993 and 1999, respectively.

In 1995, he was with the Research Institute for Electromagnetism and Electronic Components of the Italian National Council of Research (IRECE-CNR), Naples. From 1999 to 2000, he was with Telespazio S.p.A., Rome, Italy. From 2000 to 2004, he was a Research Scientist with the Department of Electronic and Telecommunication Engineering, University of Naples Federico II. He is currently a Professor of electromagnetics with the Department of Electrical Engineering and Information Technology, University of Naples Federico II. He has been involved as a Principal Investigator or a Coinvestigator in several projects funded by the European Union (EU), the Italian Space Agency (ASI), the Italian Ministry of Education and Research (MIUR), Campania Regional Government, and private companies. His main research interests include microwave remote sensing and electromagnetics, with particular focus on the modeling of electromagnetic scattering from natural surfaces and urban areas, simulation and processing of SAR signals, and electromagnetic propagation in urban areas. He is an author or a coauthor of about 300 papers, of which about 70 were published on refereed journals and the others on proceedings of international and national conferences.

Dr. Iodice received the Sergei A. Schelkunoff Prize Paper Award from the IEEE Antennas and Propagation Society in 2009, for the best paper published in 2008 in the *IEEE TRANSACTIONS ON ANTENNAS AND PROPAGATION*. He is the Chair of the IEEE South Italy Geoscience and Remote Sensing Chapter.